FEA based impedance method for designing active structures

Andrew G. Littlefield, James A. Fairweather, Kevin C. Craig
Rensselaer Polytechnic Institute, Troy, NY 12180

ABSTRACT

The impedance method predicts the response of a structure to piezoelectric patch actuators. The drawback has always been that the structure's impedances had to be calculated analytically. This work uses finite element analysis (FEA) to generate the structure's impedances from eigenvectors. This approach allows for the method to be applied to a much wider variety of structures than before, as for many structures of interest the necessary closed form expressions do not exist. At present, the method has been used with two-dimensional structures, though it should be extendable to any structure that can be accurately modeled by FEA. From a single finite element run, multiple actuator and response locations can be examined.

The equations to recover the impedances and structure's response from a FEA normal mode analysis are developed. The method is then experimentally verified for plates with different boundary conditions, material types, and actuator orientations. Comparisons are made between calculating the impedances using just the eigenvectors at the center points of the patch sides and using a shape function to describe the eigenvectors along the patch sides. The method is found to accurately predict the plate's response. In several cases the predicted response fell within the range of experimentally recovered responses.

1. INTRODUCTION

With the increased use of induced strain actuators, such as piezoelectric ceramics (PZT), comes the demand for more accurate and usable modeling methods. For a method to be effective, it must be easy to use, capture the dynamics of the physical system, and yield accurate predictions of the system's dynamic response. Until recently, all of the methods have failed to meet some or all three of these requirements. The available methods for modeling PZT actuators include the static equivalent force (SEF) method [1 2 3 4], finite element methods (FEM), [5 6 7] methods derived from first principles [7 8 9] and the impedance method.[2 10 11 12]

SEF methods are widely used due to their easy formulation and retention of physical insight into the system. They have been shown to significantly miscalculate the system's resonant frequencies, and the actuator force, stress, and strain. [2 4] No attempt is made to include the stiffness, mass or frequency response of the actuator in the model.

There are numerous ways to include PZT actuators in finite element analysis (FEA) models. Some FEM codes, such as ABAQUS, Ansys, and ATILA, have built in capability to handle PZT actuators. For those commercial codes that do not provide piezoelectric elements or to tailor the element to the application, the PZT's properties have been included into the FEA program directly through custom elements. [5 6 7] Another approach is to incorporate the excitation as a local thermal expansion. [7 13 14] This is only useful for a static case unless the FEA package has harmonic thermal expansion analysis. While FEM is accurate, it can be very computationally expensive when testing multiple actuator locations and there is often a loss of physical insight into the system.

The use of first principles can allow for both the mechanical and electrical aspects of the actuator to be taken into account. Which aspects and to what degree, depend upon the principle applied. Among the principles used are the Rayleigh-Ritz energy method [7 8] and Bernoulli-Euler beam theory.[9] The drawback to this approach is that for anything more complex than a simple beam these models become very high order. This makes them ill suited for typical design studies, such as optimal placement of actuators. Additionally, the dynamics of the structure and actuator are solved simultaneously, so for every change in actuator placement, the whole problem must be solved again.

Of the methods mentioned, only the impedance method, as developed at Virginia Polytechnic Institute [2], comes close to meeting all three requirements. The mechanical impedance of the host structure is used to determine the load at the actuator boundary. This is then used to determine the dynamic response of the system and actuator. These models have been shown to have very good agreement with experimental results.[4 15] The approach can even recover the response at the nodal lines, which is something that the SEF method cannot.

An advantage of this method is that since the structure's impedance is found independent of the actuator, it is easy to try out different actuator locations. The major drawback to this method is the determination of the structure's mechanical impedances. These are found by analytically solving the structure's vibration problem. This limits the methods applicability to simple geometries for which a closed form solution of the impedance can be found.

The technique presented in this paper uses FEA to generate the structure's impedances. This approach extends the impedance method to any structure that can be accurately modeled by FEA. Fairweather [16] first developed and experimentally verified this for beams. For plates he laid out the equations and compared the predictions to previously published experimental data. A more detailed experimental investigation was needed to verify the predictive capability of the technique.

First, the equations to recover the impedances and structure's response from a FEA normal mode analysis will be developed. Then the method will be experimentally verified for plates with different boundary conditions, material types, and actuator orientations. Comparisons will be made between calculating the impedances using just the eigenvectors at the center points of the patch sides and using a shape function to describe the eigenvectors along the patch sides. The experimental results will then compared to the theory.

2. MODELING OF THE PIEZOELECTRIC CERAMIC PATCH

Zhou [4] gives a detailed derivation of the solution for the actuator's vibration problem. The moments and forces the PZT patch applies to the structure are expressed in terms of the structure's impedances. Rather than just reiterate their work only the main points will be presented here.

The following assumptions are made for the PZT actuator:

- It undergoes an extensional vibration in two dimensions.
- The electrical field applied to the actuator is spatially uniform over the electrodes of the patch.
- The material is isotropic in the x-y plane.

The equations of motion are found by summing the stresses on a two dimensional differential element. Using the above assumptions and using the constitutive equations to express the stresses, Zhou [4] came up with the following equations of motion:

$$\frac{Y^E}{1-n_p^2}\frac{\partial^2 u}{\partial x_p^2}+\frac{Y^E}{2(1-n_p)}\frac{\partial^2 v}{\partial x_p \partial y_p}+\frac{Y^E}{2(1+n_p)}\frac{\partial^2 u}{\partial y_p^2}=r_p\frac{\partial^2 u}{\partial t^2}, \tag{1}$$

$$\frac{Y^E}{1-n_p^2}\frac{\partial^2 v}{\partial y_p^2}+\frac{Y^E}{2(1-n_p)}\frac{\partial^2 u}{\partial x_p \partial y_p}+\frac{Y^E}{2(1+n_p)}\frac{\partial^2 v}{\partial x_p^2}=r_p\frac{\partial^2 v}{\partial t^2}, \tag{2}$$

where Y^E is the patch's modulus of elasticity, n_p is its Poisson's ratio, u is its displacement in the x direction, v is its displacement in the y direction, and r_p is its density.

These coupled equations describe a classical problem in elasticity, one that was shown by Love [17] to have a complete analytical solution if the material domain is bounded by a circle.

However in this case we have a rectangular or square patch. This complicates the solution. Also the boundary conditions are in terms of the structure's impedances. Zhou [4] solved this problem by neglecting the change of rate of shear strain terms. This reduces the equations to:

$$\frac{Y^E}{1-{n_p}^2}\frac{\partial^2 u}{\partial {x_p}^2} = r_p \frac{\partial^2 u}{\partial t^2}, \tag{3}$$

$$\frac{Y^E}{1-{n_p}^2}\frac{\partial^2 v}{\partial {y_p}^2} = r_p \frac{\partial^2 v}{\partial t^2}, \tag{4}$$

which can then be solved by separation of variables with an assumed solution of:

$$u(x_p,t) = f(x_p)q(t) = \left(A\sin\left(\Omega x_p\right) + B\cos(\Omega x_p)\right)e^{jwt}, \tag{5}$$

$$v(y_p,t) = f(y_p)q(t) = \left(C\sin\left(\Omega y_p\right) + D\cos(\Omega y_p)\right)e^{jwt}, \tag{6}$$

where Ω is the spatial frequency of the oscillations.

The boundary conditions of the piezoceramic patch are:

$$u(0,t) = 0 \quad v(0,t) = 0, \tag{7}$$

which leads to $B = D = 0$.

A and C can then be found by substituting the assumed solution into the constitutive equations with the stresses expressed in terms of the structure's impedances. This constitutive equation is:

$$\begin{bmatrix} \frac{\partial u}{\partial x_p} \\ \frac{\partial v}{\partial y_p} \end{bmatrix} = -\frac{1}{\tilde{Y}_{11}^E}\begin{bmatrix} 1 & -n_p \\ -n_p & 1 \end{bmatrix}\begin{bmatrix} \frac{1}{A_x} & 0 \\ 0 & \frac{1}{A_y} \end{bmatrix}\begin{bmatrix} Z_{xx} & Z_{xy} \\ Z_{yx} & Z_{yy} \end{bmatrix}\begin{bmatrix} \dot{u} \\ \dot{v} \end{bmatrix} + \begin{bmatrix} d_{31} \\ d_{32} \end{bmatrix}E_3, \tag{8}$$

where E_3 is the applied electric field.

When (5) and (6) are substituted into this and evaluated at $x_p = a_p$ and $y_p = b_p$ one obtains:

$$\begin{bmatrix} A \\ C \end{bmatrix} = \begin{bmatrix} \Omega\cos(\Omega a_p) + \frac{jwZ_{xx}\sin(\Omega a_p)}{Y^E A_x} - \frac{jwn_p Z_{yx}\sin(\Omega a_p)}{Y^E A_y} & \frac{jwZ_{xy}\sin(\Omega b_p)}{Y^E A_x} - \frac{jwn_p Z_{yy}\sin(\Omega b_p)}{Y^E A_y} \\ \frac{jwZ_{yx}\sin(\Omega a_p)}{Y^E A_y} - \frac{jwn_p Z_{xx}\sin(\Omega a_p)}{Y^E A_x} & \Omega\cos(\Omega b_p) + \frac{jwZ_{yy}\sin(\Omega b_p)}{Y^E A_y} - \frac{jwn_p Z_{xy}\sin(\Omega b_p)}{Y^E A_x} \end{bmatrix}^{-1}\begin{bmatrix} d_{31} \\ d_{32} \end{bmatrix}E_3, \tag{9}$$

These expressions correct those presented by Zhou.[4] The Z_{ij} are the impedances of the structure. Using them and the assumed displacement solutions, (5) and (6), the force output in terms of the impedance of the mechanical structure is:

$$\begin{bmatrix} F_{a_p} \\ F_{b_p} \end{bmatrix} = -jw\begin{bmatrix} Z_{xx} & Z_{xy} \\ Z_{yx} & Z_{yy} \end{bmatrix}\begin{bmatrix} A\sin(\Omega a_p) & 0 \\ 0 & C\sin(\Omega b_p) \end{bmatrix}e^{jwt}, \tag{10}$$

where coefficients A and C are given by (9). The moment exerted by the patch on the structure is found by using the geometric relationship between force and moment:

$$\begin{bmatrix} M_{a_p} \\ M_{b_p} \end{bmatrix} = -jw\left(t_p + h_p\right)\begin{bmatrix} Z_{xx} & Z_{xy} \\ Z_{yx} & Z_{yy} \end{bmatrix}\begin{bmatrix} A\sin(\Omega a_p) & 0 \\ 0 & C\sin(\Omega b_p) \end{bmatrix}e^{jwt}. \tag{11}$$

Now that the force and moment exerted by the PZT patch has been determined in terms of the host structure's mechanical moment impedance, the mechanical moment impedances themselves must be determined.

3. DETERMINATION OF THE MOMENT IMPEDANCES FROM FEA

Since the impedances are to be determined using MSC/Nastran, the next step is to develop a means to extract the frequency response functions from MSC/Nastran. To do this it is necessary to develop a relationship between the eigenvectors of a node and the forces, moments, velocities and displacements associated with that node.

Consider the following sets of undamped spring mass systems:

$$[M]\ddot{\mathbf{x}} + [K]\mathbf{x} = \mathbf{f(t)}, \tag{12}$$

where $\mathbf{x}$ and $\mathbf{f(t)}$ are (n x 1) vectors describing the physical positions and time varying forcing functions applied to each degree of freedom of the system. Assume that:

- Mass matrix is non-singular.
- Mass and stiffness matrices are symmetric.

Taking the equation to the Laplace domain yields:

$$[M]s^2\mathbf{X(s)} + [K]\mathbf{X(s)} = \mathbf{F(s)}. \tag{13}$$

Define a set of eigenvalues, $[\Lambda]$, and mass-normalized eigenvectors, $[\Phi]_n^T$, such that:

$$\mathbf{Q}(s)s^2 - [\Lambda]\mathbf{Q(s)} = [\Phi]_n^T\mathbf{F(s)}. \tag{14}$$

The motion of the system in the physical coordinate system can be obtained through the coordinate transformation,

$$\mathbf{X}(s) = [M]^{-\frac{1}{2}}[\Phi]\mathbf{Q}(s) = [\Phi]_n\mathbf{Q}(s), \tag{15}$$

so that:

$$\mathbf{X}(s) = [\Phi]_n\left([I]s^2 - [\Lambda]\right)^{-1}[\Phi]_n^T\mathbf{F(s)}. \tag{16}$$

This is the equation relating the displacement vector in physical coordinates to force applied in physical coordinates. For a specific physical coordinate $X_j(s)$ and force $F_k(s)$:

$$\frac{X_j(s)}{F_k(s)} = \sum_{i=1}^{\infty}\frac{[\Phi(j,i)]_{n_X}[\Phi(k,i)]_{n_F}}{s^2 + w_i^2}. \tag{17}$$

Differentiating (17) yields the mechanical admittance, the inverse of the mechanical impedance, of the structure:

$$\frac{V_j(s)}{F_k(s)} = \sum_{i=1}^{\infty}\frac{[\Phi(j,i)]_{n_X}[\Phi(k,i)]_{n_F}\,s}{s^2 + w_i^2}. \tag{18}$$

This equation for the mechanical admittance makes no requirements on the type of structure, so it can be used for any structure. Since we are interested in plates, we will now show how to get the moment impedances for a plate from (18).

Consider the following diagram of the piezoceramic patch attached to a plate structure.

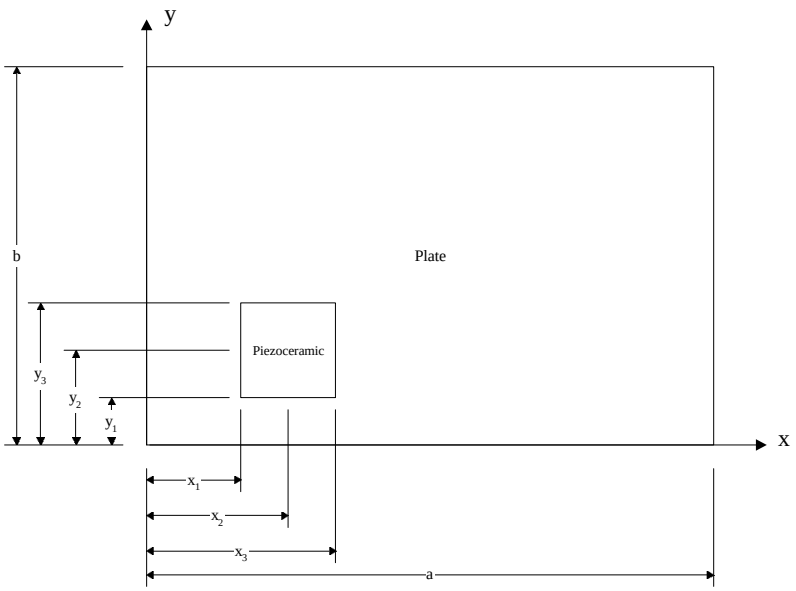

Figure 1: Schematic drawing showing size of plate and location of patch

Inserting the eigenvectors associated with rotation for both the force input and velocity output into (21), one obtains the transfer function between rotational velocity and applied moment. For example, if the eigenvectors associated with rotation about the y-axis at (x_1, y_2) are substituted for both the input and output, one obtains a moment admittance about the y-axis of the structure at the center of the left edge of the patch:

$$\frac{sq_{(x_1,y_2)}(s)}{m_{(x_1,y_2)}(s)} = \sum_{i=1}^{\infty} \frac{\left[\Phi\left(R2_{(x_1,y_2)},i\right)\right]_{n_X}\left[\Phi\left(R2_{(x_1,y_2)},i\right)\right]_{n_F} s}{s^2+w_i^2}. \tag{19}$$

Using the principal of superposition, one can obtain the admittance transfer function between the differential rotational velocity about the y-axis at points (x_1, y_2) and (x_3, y_2) and counter-posed moments applied at the same points as

$$\frac{s\left[q_{(x_1,y_2)}(s)-q_{(x_3,y_2)}(s)\right]}{\left[m_{(x_1,y_2)}(s)-m_{(x_3,y_2)}(s)\right]} = \sum_{i=1}^{\infty} \frac{\left[\Phi\left(R2_{(x_1,y_2)},i\right)-\Phi\left(R2_{(x_3,y_2)},i\right)\right]_{n_X}\left[\Phi\left(R2_{(x_1,y_2)},i\right)-\Phi\left(R2_{(x_3,y_2)},i\right)\right]_{n_F} s}{s^2+w_i^2} = H_{xx}. \tag{20}$$

The other H_{ij} are found in a similar fashion and a matrix equation relating differential rotational velocities to the mechanical moment admittances and applied counter-posed moments is written as:

$$\begin{bmatrix} s\Delta q_x(s) \\ s\Delta q_y(s) \end{bmatrix} = \begin{bmatrix} H_{xx} & H_{xy} \\ H_{yx} & H_{yy} \end{bmatrix} \begin{bmatrix} \Delta m_x(s) \\ \Delta m_y(s) \end{bmatrix}. \tag{21}$$

Using geometrical relationships (21) can be rewritten to give the applied force as:

$$\begin{bmatrix} \Delta F_{x_p}(s) \\ \Delta F_{y_p}(s) \end{bmatrix} = \frac{2}{\left(t_p+h_a\right)^2} \begin{bmatrix} H_{xx} & H_{xy} \\ H_{yx} & H_{yy} \end{bmatrix}^{-1} \begin{bmatrix} s\Delta u(s) \\ s\Delta v(s) \end{bmatrix}, \tag{22}$$

where t_p is the thickness of the plate and h_a is the thickness of the actuator.

The structure's moment impedances are then given as:

$$\begin{bmatrix} Z_{xx} & Z_{xy} \\ Z_{yx} & Z_{yy} \end{bmatrix} = -\frac{2}{(t_p + h_a)^2} \begin{bmatrix} H_{xx} & H_{xy} \\ H_{yx} & H_{yy} \end{bmatrix}^{-1} = \begin{bmatrix} Q_{xx} & Q_{xy} \\ Q_{yx} & Q_{yy} \end{bmatrix}^{-1}, \tag{23}$$

where Q_{kl} is defined to be the in plane force admittance.

Utilizing the preceding results the moments exerted by the piezoceramic can be computed from (11) based on the impedances given in (23).

4. DETERMINATION OF THE STRUCTURE'S RESPONSE

Now that we have the structure's impedances in terms of its eigenvalues and eigenvectors, we need to develop an equation that will give us the displacement in the z-direction. The vibration response of the plate in terms of eigenvectors is given as:

$$w(x, y, t) = \sum_{m=1}^{\infty} \sum_{n=1}^{\infty} \frac{F_{mn} f_{mn}(x, y)_n}{\left(w_{mn}^2 - w^2\right)} Q_t e^{jwt}, \tag{24}$$

where Q_t is the temporal amplitude, which is assumed to be unity, and $f_{mn}(x, y)_n$ are the mass normalized eigenvectors. F_{mn} is the modal force projection and is given as:

$$F_{mn} = -\overline{M}_x \int_{y_1}^{y_3} \left(-\frac{\partial f_{mn}(x, y)_n}{\partial x}\bigg|_{x=x_1} + \frac{\partial f_{mn}(x, y)_n}{\partial x}\bigg|_{x=x_3} \right) dy - \overline{M}_y \int_{x_1}^{x_3} \left(-\frac{\partial f_{mn}(x, y)_n}{\partial y}\bigg|_{y=y_1} + \frac{\partial f_{mn}(x, y)_n}{\partial y}\bigg|_{y=y_3} \right) dx. \tag{25}$$

The moments in terms of the structure's impedances are given by (11). To perform this integration it is necessary to have an expression for the spatial derivatives of the eigenvectors in the domains of interest. Under the Kirchoff hypothesis, the spatial derivatives are the rotational eigenvectors R1 and R2:[18]

$$R1 = -\frac{\partial f(x, y)_n}{\partial y}, \tag{26}$$

$$R2 = \frac{\partial f(x, y)_n}{\partial x}. \tag{27}$$

MSC/Nastran reports these at the nodes along the edge of the actuator, so they are fit to a sixth order polynomial so that the integration can be carried out explicitly.

The polynomial can then be integrated to obtain the individual modal force projection in terms of $\overline{M}_x$ and $\overline{M}_y$:

$$w(x, y, t) = \sum_{m=1}^{\infty} \sum_{n=1}^{\infty} \frac{\left(E_{x_n} \overline{M}_x + E_{y_n} \overline{M}_y\right) f_{mn}(x, y)_n}{\left(w_{mn}^2 - w^2\right)} e^{jwt}, \tag{28}$$

where E_{x_n} and E_{y_n} are the results of the spatial integration of the rotations about the x-axis and y-axis respectively.

For actuators at an angle to the structure's axis the eigenvectors must be modified. MSC/Nastran reports the eigenvectors in the global coordinate system. The expressions for the force and moments exerted by the patch, as presented in Section 2 are expressed in the patch's coordinate system. So the eigenvectors have to be rotated from the global system of the plate to the patch's own coordinate system. Since the Z-axis is the same for both the patch and the plate there is no need to rotate any of the Z quantities back to the global system to find the transverse displacement.

The moment impedances found in Section 3 all use eigenvectors from only the center of the patch sides. This single point may not be a good representation of the entire side of the patch. A better result may be possible by using the entire side of the patch to calculate the moment impedance. As was the case with the modal force projection, we only know the eigenvectors at the nodes, which are discrete points. The same approach is employed as was used with the modal force projection. In fact, the same polynomial used for the modal force projection can be used in computing the impedances. This allows the use of shape functions for calculating the impedances without any extra work.

5. FEA MODELS

The first step in testing the method is to generate accurate FEA models. Since the method relies on the eigenvectors generated from an FEA model to calculate the impedances, it is important that the model be as accurate as possible. Any errors in the FEA model will cause the final results to be in error.

The models were generated in FEMAP and then run in MSC/NASTRAN. The first model made was for a 6061-T6-aluminum plate bolted at all four corners. CQUAD4 elements were used to model the plate and a normal mode analysis was run to extract the first 35 modes. To make sure that this model accurately represents the plate a modal analysis of the actual plate was conducted with an impact hammer. The experimental setup is shown in Figure 2.

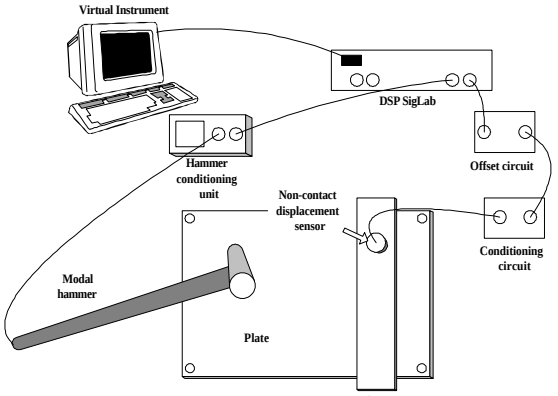

Figure 2: Modal Testing of the Plate

The experimentally recovered modes were then compared to the modes from the FEA model. The difference between the experimental and FEA modes is shown in Table 1

Table 1 Difference between Predicted and measured Modes

Mode	Measured Frequency (rad/sec)	Predicted Frequency (rad/sec)	Percent Difference
1	81.8750	81.40003	-0.58%
2	137.5000	137.2957	-0.15%
3	210.6250	205.8459	-2.27%
4	240.6250	234.2385	-2.65%
5	334.3750	329.3206	-1.51%
6	338.7500	332.9155	-1.72%
7	356.2500	348.4398	-2.19%

This was deemed to be an acceptable fit, so the final models with the different boundary conditions could be made. There were three sets of boundary conditions, one with bolts on four corners, a second with the four bolts plus two additional bolts in the interior, and a third with the holes for the interior bolts but no constraints on the holes. The final models consisted of both CQUAD4 and CTRIA3 elements. The CTRIA3 elements were used when the aspect ratio of the CQUAD4 elements became unacceptable.

The same procedure was followed for the composite plates. The plates were made out of a graphite cloth with a lay up of $[0/90, +45/-45]_s$. The initial results of the modal testing were very unsatisfactory. Differences were found on the order of 50%. It was discovered that the quoted properties for the graphite were for a unidirectional prepreg, whereas the material used was a bi-directional cloth used in a wet lay-up. Due to time constraints the only material value that could be experimentally obtained was a bending modulus for the laminate. This result was used in FEMAP and the laminate was entered as 2-D orthotropic material instead of as individual plies. The final results for the modal testing are shown in Table 2.

Table 2 Difference between Predicted and measured Modes

Mode	Measured Frequency (rad/sec)	Predicted Frequency (rad/sec)	Percent Difference
1	65.5357	65.7899	0.39%
2	111.7708	110.595	-1.06%
3	130.4167	166.8	21.81%
4	175.0000	188.9572	7.39%
5	224.6429	266.1453	15.59%
6	276.9906	267.9463	-3.38%
7	294.1667	282.0647	-4.29%

These results were not as good as those for the aluminum plate but were the best that could be obtained without having better material property data. As in the case of the aluminum plate, there were three sets of boundary conditions, one with bolts on four corners, a second with the four bolts plus two additional bolts in the interior, and a third with the holes for the interior bolts but no constraints on the holes. The final models again consisted of both CQUAD4 and CTRIA3 elements.

6. EXPERIMENTS AND RESULTS

Four aluminum and two composite plates were made. Two of the aluminum plates had PZT patches aligned with the plate's axis and two had patches at 45 degrees to the plate's axis. For the composite plates there was one aligned and one at 45 degrees. Initially all plates had four holes drilled at the corners and were bolted down at these points. The experimental setup can be seen in Figure 3.

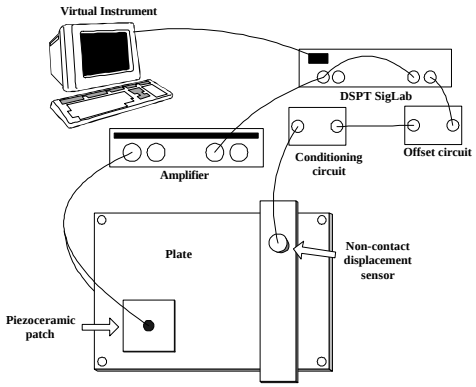

Figure 3: Experimental setup

The patches were excited with a sine wave generated by the sine sweep analyzer of a DSPT SigLab. This signal was then passed through an amplifier with a fixed gain of 20. The sine sweep bands and excitation voltages were varied so as to get a good response at each of the first six or so modes. The exact band settings and voltages varied from plate to plate. An eddy current sensor measured the response of the plate and SigLab computed the transfer function. The sensor was located at x = 0.2032m and y = 0.1524m as measured from the origin shown in Figure 1. For the composite plate, a button of aluminum was glued to the plate so that the sensor could be used. This button was also added to the FEA model.

Each plate was run twice with just the four corners bolted down. All four bolts were tightened to a torque of 10 ft/lbs. This was done to avoid any moments that would be introduced into the plate by uneven tightening of the bolts. After running the tests in the initial configuration, the plates were removed and the interior holes were drilled. The interior bolts were also tightened to a torque of 10 ft*lbs. Two runs for each plate were done in this configuration. Two final runs were done on each plate without the interior bolts but with the interior holes.

After collecting all of the data, the experimental transfer functions were then compared to the ones predicted by the method. Several MATLAB m-files were created for this purpose and comparisons were made between evaluating the eigenvectors at the center points versus using shape functions.

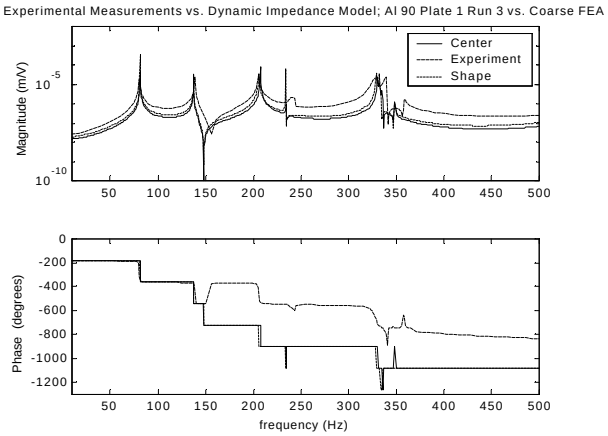

Figure 4: Aluminum plate with 90-degree patch

Figure 4 shows the experimental versus predicted results for an aluminum plate with a patch aligned with the plate's axis. As can be seen from the plots there is very little difference between using the eigenvectors at the center points of the patch sides and using shape functions to describe the eigenvectors along the patch sides. For the first pole both methods are within 1% of the experimentally found ones. For the second pole they are within 2%. In both cases the difference between measured and predicted is of a similar magnitude as the differences between experimental runs. The differences between the two methods are the magnitudes of the poles. The locations of the poles remain the same in both approaches.

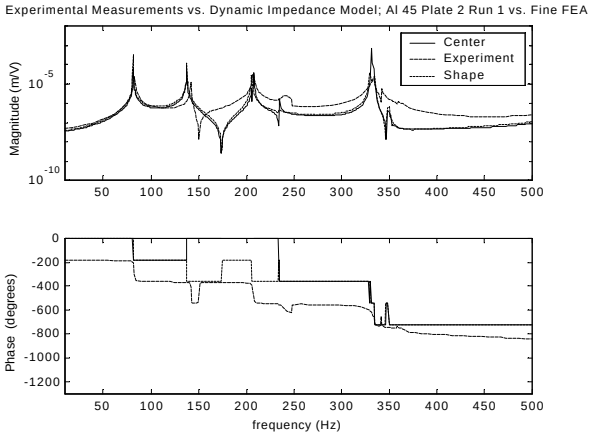

Figure 5: Aluminum plate with 45-degree patch

Figure 5 shows the experimental versus predicted results for an aluminum plate with a patch at 45 degrees to the plate's axis. Like the 90-degree case there is practically no difference in predicting the poles between the methods. For the first pole the difference was 2%. For the second pole it was 3%. Though this seems like a larger range than the 90-degree case, the range is due to differences between experimental runs and not predictions. There is one difference between the methods that was not seen in the 90-degree case. Though it is not readily apparent from the figure, the center point approach predicts extra

poles and zeroes that the shape function approach does not. These “extra” poles and zeroes are not found experimentally. By averaging the force application along the edge of the actuator, better prediction of the physical response is achieved.

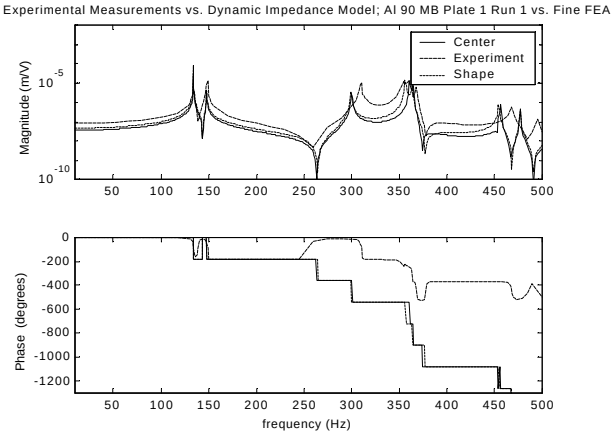

Figure 6: Aluminum plate with 90-degree patch and interior bolts

Figure 6 shows the results for an aluminum plate with a patch aligned with the plate's axis and having interior bolts. There is little difference between the center point and shape function approaches. For the first two poles both methods are less than 1% from the measured pole locations. The shape function approach predicts slightly larger magnitudes and earlier poles and zeroes for the higher frequency modes. Both approaches under predict the pole at 300 Hz by about 5 Hz. However, the shape function approach correctly predicts the next pole, whereas the center point approach misses it by several Hz.

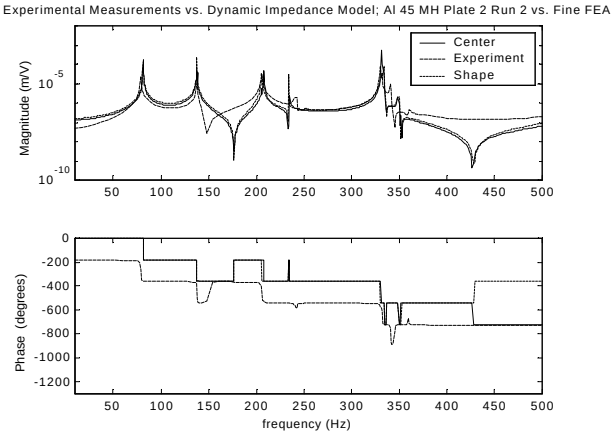

Figure 7: Aluminum plate with 45-degree patch and interior holes

Figure 7 shows the results for an aluminum plate with a patch at 45 degrees to the plate's axis with interior holes. As would be expected this result is very similar to that seen in Figure 5. Both approaches do a good job of following the trend of the experimental response. Both approaches were off by 3 % for the first pole and less than 1% for the second pole. The use of shape functions does give a better prediction of the magnitude though in most cases the difference between the two approaches is negligible.

As was seen with the other 45-degree case, the center point approach predicts extra pairs of poles and zeroes not seen in the shape function approach. These may arise from the rotation of the eigenvectors. Since the shape function approach fits the eigenvectors to a polynomial after the rotation these effects are most likely averaged out.

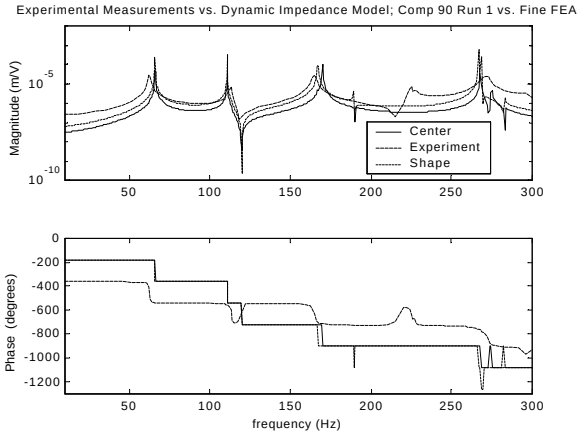

Figure 8: Composite plate with 90-degree patch

The results for a composite plate with its actuator aligned with the plate's axis are shown in Figure 8. Overall the predicted response shows the same trends as the experimental results. The agreement is quite good below 175 Hz. To this point the curves lie almost on top of each other. Both approaches were off by 4.5% for the first pole and by 2% for the second one. This difference is within the variation seen between experimental runs. For the third pole the shape function approach is off by 1 % whereas, the center point approach is off by 3%. The next pole though is under predicted by about 20% by the shape function approach and completely missed by the center point approach. This could be due to the errors in the higher modes in the underlying FEA model.

7. SUMMARY

For a modeling method to be useful it must not only give an accurate prediction, but also be easy to use and retain a physical insight into the system. Until recently, all the methods of modeling piezoceramic actuators are were lacking in one or more of these areas.

SEF models are the easiest to use and they still retain a physical insight into the system but are not very accurate. FEA models are accurate, but require training in specific programs or the ability to write your own custom elements. Also, physical insight can become obscured. First principles give accurate models and retain physical insight. However, for anything more complex than a simple beam these models become very high order, which makes them ill suited for typical design studies.

Impedance methods are accurate and retain insight, but until recently, they have relied on finding the impedances analytically. This has limited their use to structures for which this can be done, such as beams, curved shells, and plates. Even then, with these simple structures, only certain boundary conditions could be solved for. Fairweather[16] developed a method whereby the impedances could be found from FEA. He calculated the response for a beam and compared his results to experimental measurements. For plates he presented the equations and compared the results to the SEF method.

There were several issues left open, though, that had to be addressed before the method was ready for general use. These were the use of different boundary conditions, material symmetries, methods of computing the applied moment, and off axis actuator placement. Experimental data to corroborate the predictions was also needed.

In this work the necessary equations were developed and it was shown what modifications were needed to allow for off axis actuators and to use shape functions instead of center points calculations for the impedances. The creation and validation of the FEA models, without actuators was covered. Finally the experimental results were presented.

The results show good agreement between the predicted and measured response of the plate. In most cases there is little or no difference between the shape functions and center point approaches. When there is though it is the shape function calculations that give the better results. They give better off resonance magnitudes than center point calculations and do not

predict extra pole zero pairs like the center point ones. Since they require no extra work, it is advisable to use them whenever possible.

The results are similar no matter what boundary condition or material symmetry. For off axis actuators, the only difference comes with the center point approach. With it extra pole / zero pairs are predicted when the actuator is not aligned with the plate's axis. These reasons are cited as motivation to use the shape function approach.

Taken altogether these results show that by obtaining the impedances from FEA, the impedance method can be applied to large range of structures. The equations presented should remain valid for any section of a structure that can be modeled using plate elements. Since the actuator is not in the FEA model, the designer is free to try multiple actuator and response locations without having to rerun the FEA analysis.

REFERENCES

1. Crawley, E. F., and de Luis, J., 'Use of Piezoelectric Actuators as Elements of Intelligent Structures," *AIAA Journal*, Vol. 25, No. 10, 1987, pp. 1373 - 1385.
2. Liang, C., Sun, F.P., and Rogers, C.A., "An Impedance Method for Dynamic Analysis of Active Material Systems," Collection of Technical Papers- AIAA/ASME Structures, Structural Dynamics, and Materials Conference from the 34th AIAA/ASME/ASCE/AHS/ASC Structures, Structural Dynamics, and Materials Conference, 1993b, pp. 3587-3599.
3. Lalande, F., "Modeling of the Induced Strain Actuation of Shell Structures," Doctoral Thesis, Virginia Polytechnic Institute, 1995.
4. Zhou, S., Liang, C., and Rogers, C.A., "An Impedance-Based System Modeling Approach for Induced Strain Actuator-Driven Structures," *Journal of Vibration and Acoustics*, Vol. 118, July 1996, pp. 323-331.
5. Allik, H., and Hughes, T. J. R., "Finite Element Method for Piezoelectric Vibration," *International Journal for Numerical Methods in Engineering*, Vol. 2, 1970, pp. 151 - 157.
6. McDearmon, G. F., "The Addition of Piezoelectric Properties to Structural Finite Element Programs by Matrix Manipulations," *Journal of the Acoustic Society of America*, Vol. 76, No. 3, Sep 1984, pp. 666 - 669.
7. Hagood, N. W., Chung, W. H., and von Flotow, A, "Modeling of Piezoelectric Actuator Dynamics for Active Structural Control." *Journal of Intelligent Material Systems and Structures*, Vol. 1, Jul 1990, pp. 327 - 354.
8. Akella, P., Chen, X., Cheng, W., Hughes, D., Wen, J., "Modeling and Control of Smart Structures with Bonded Piezoelectric Sensors and Actuators," *Smart Materials and Structures*, Vol. 3, 1994, pp. 344-353.
9. Pan J., Hansen C.H., Snyder S.D., "A Study of the Response of a Simply Supported Beam to Excitation by a Piezoelectric Actuator," *Recent Advances in Active Control of Sound and Vibration*, edited by Fuller C.R., Rogers C.A., Virginia Polytechnic Institute, 1991, pp. 39-49.
10. Liang, C., Sun, F.P., Rogers, C.A., "Dynamic Output Characteristics of Piezoelectric Actuators," *SPIE*, Vol. 1916, 1993a, pp. 341-352.
11. Zhou S. Liang C., and Rogers C.A., "Impedance Modeling of Two-Dimensional Piezoelectric Actuators Bonded on a Cylinder," edited by Carman, G.P., and Garcia, E., *Adaptive Structures and Material Systems*, AD- Vol.35, 1993 ASME Winter Annual Meeting, New Orleans, La., Nov. 28 - Dec. 3, 1993, pp. 247-255.
12. Zhou, S., Liang, C., and Rogers, C.A., "A Dynamic Model of Piezoelectric Actuator-Driven Thin Plates," *Proceeding of the Smart Structures and Materials Conference*, Orlando, SPIE Vol. 2190, 1994, pp. 550-562.
13. Liang, C., and Rogers, C.A., "Behavior of Shape Memory Alloy Actuators Embedded in Composites," *Proceedings of the 1989 International Composites Conference*, Beijing, China, 1-4 Aug. 1989, pp. 475-482.
14. Ha, S. K., Keilers, C., and Chang, F., "Finite Element Analysis of Composite Structures Containing Distributed Sensors and Actuators," *AIAA Journal*, Vol. 30, No. 3, Mar 1992.
15. Mollenhauer, D.H., Hayden-Griffin, O., "Induced Strain Actuation of Surface Bonded Piezoceramic Patches: A Numerical and Experimental Study," *Journal of Intelligent Material Systems and Structures*, Vol. 5, May 1994, pp. 355-362.
16. Fairweather, James, "Designing with Active Materials: an Impedance Based Approach," Doctoral Thesis, Rensselaer Polytechnic Institute, 1998.
17. Love, A.E.H., A Treastise on the Mathematical Theory of elasticity, Dover Publications, 4th Edition, New York, 1944.
18. MacNeal, R.H., Finite Elements: Their Design and Performance, Marcel Dekker, Inc., New York, 1994.